

# Meaningful representations emerge from Sparse Deep Predictive Coding

Victor Boutin<sup>a,b,\*</sup>, Angelo Franciosini<sup>a</sup>, Franck Ruffier<sup>b</sup>, Laurent Perrinet<sup>a</sup>

<sup>a</sup>*Aix Marseille Univ, CNRS, INT, Inst Neurosci Timone, Marseille, France*

<sup>b</sup>*Aix Marseille Univ, CNRS, ISM, Marseille, France*

---

## Abstract

Convolutional Neural Networks (CNNs) are the state-of-the-art algorithms used in computer vision. However, these models often suffer from the lack of interpretability of their information transformation process. To address this problem, we introduce a novel model called Sparse Deep Predictive Coding (SDPC). In a biologically realistic manner, SDPC mimics how the brain is efficiently representing visual information. This model complements the hierarchical convolutional layers found in CNNs with the feed-forward and feed-back update scheme described in the Predictive Coding (PC) theory and found in the architecture of the mammalian visual system. We experimentally demonstrate on two databases that the SDPC model extracts qualitatively meaningful features. These features, besides being similar to some of the biological Receptive Fields of the visual cortex, also represent hierarchically independent components of the image that are crucial to describe it in a generic manner. For the first time, the SDPC model demonstrates a meaningful representation of features within the hierarchical generative model and of the decision-making process leading to a specific prediction. A quantitative analysis reveals that the features extracted by the SDPC model encode the input image into a representation that is both easily classifiable and robust to noise.

*Keywords:* Convolutional hierarchical network, Unsupervised learning, Feature extraction, Sparse coding, Predictive coding, Meaningful features.

---

<sup>\*</sup>Corresponding author: victor.boutin@univ-amu.fr

## 1. Introduction

Artificial Neural Networks (ANNs) were introduced more than half a century ago to provide a biologically-inspired computational framework in alternative to the classical Von-Neuman computer architecture. More recently, Deep Learning (DL) approaches have grown out of the bio-inspired roots of ANNs to become the state-of-the-art machine learning method [1]. In DL, the ANN defines a generic input-output function as a series of stacked non-linearities [2] whose numerous parameters can be progressively modified to best learn a fit between the input and output. Recent practical examples show the universality of these ANNs in approximating arbitrary functions. Convolutional Neural Networks (CNNs), a particular class of ANNs, have consistently overtaken most of other computer vision algorithms in a wide variety of problems such as: feature extraction [3], classification [4], detection [5] or segmentation [6]. However, as CNNs are becoming ubiquitous in computer vision, a recurrent criticism is rising about the relative opacity underlying their decision-making process. In particular, interpretability of CNNs becomes difficult as the number of their parameters increases. Even if recent studies have exposed new methods to visualize these parameters [7], it is still not completely understood which factors explain CNNs decisions. This problem is even more acute as this new generation of computing devices are now used in life-critical applications, such as medicine or autonomous driving.

On the contrary, biological neurons —as they are recorded in visual areas— have often interpretable properties in terms of a preference for some visual features. For instance neurons in the primary visual cortex (V1) have a preference for localized oriented edges [8]. As such, a solution to tackle the interpretability problem may consist in returning to the biological roots of ANNs. In a breakthrough study, Olshausen & Field [9] showed that neurons of V1 may be understood by decomposing an input signal (e.g. image) into a small number of competitive causes (e.g. features) through a sparse coding mechanism. Similarly, sparse coding applied to CNNs could make the decision-making process easily explained by a linear combination of a limited number of dominant causes. Sparse coding strategies have been successfully applied by neuroscientists to model some properties of the visual cortex [9, 10]. Recent advances have shown that these models are related to a wide range of mathematical methods to extract sparse representations [11], yet most often with a single processing layer. Interestingly, Predictive Coding

(PC), a theory formalized by Rao & Ballard [12] to model contextual effects in a population of V1 neurons, gives a framework to combine sparse coding with a hierarchical structure [13]. Indeed, PC suggests that the brain uses Bayesian inference to consistently update an internal model of the world that describes the possible causes of a given sensory input [14]. Whereas the vast majority of CNN are mainly feed-forward, PC introduces recurrent connections combining top-down and bottom-up processes. This PC model is able to replicate classical and extra-classical Receptive Fields (RFs) effects as measured in biology. PC suggests that top-down connections convey prediction of activity in the lower level while bottom-up processes transmit prediction error to the next higher level.

Our intuition is that by combining the hierarchy of convolutional layers employed in deep learning with the PC framework used in computational neuroscience, we could create a model capable of extracting meaningful features. Ideally, such features would describe the most informative parts of the presented image while being able to reconstruct it as faithfully as possible. These features should provide a representation of the input image allowing its identification, and even better, should be able to recover the visual signal in the image when it is degraded by noise. In this paper, we introduce a novel model called Sparse Deep Predictive Coding (SDPC). This model can be used to extract meaningful hierarchical features without any supervision. The main novelties and contributions are the following:

- We propose a model that generates image representation for machine learning by mimicking how the brain encodes visual stimuli.
- To the best of our knowledge, this is the first time that a sparse, hierarchical convolutional model is leveraged using the PC theory.
- We interpret the extracted features and representations in the context of a hierarchical generative model to visualize the decision-making process of the SDPC and show that it may provide an efficient representation of visual information.

The rest of the paper is organized as follows. In section 2, we review some studies related to SDPC. In section 3, we detail the theory that leads to the SDPC algorithm and training procedures. In section 4, we report some experimental results on two different image databases and we compare the proposed model with another relevant one. Finally, section 5 concludes the paper.

## 2. Related works

From a signal processing point of view, sparse coding holds the idea that signals (e.g. images) can be concisely described as a linear combination of a few causes (called features) drawn from a bigger set (called dictionary) [11]. Such models could be decomposed into two different but related sub-problems: inference and dictionary learning. Inference (also termed pursuit) consists in finding an accurate sparse representation of the input data, knowing the dictionary. Many algorithms (e.g. ISTA & FISTA [15], Matching Pursuit [16] or Coordinate Descent [17]) have been proposed to tackle the inference problem. Once the sparse representation has been estimated, one possible approach is to learn the set of features from the data through unsupervised dictionary learning [18, 19]. Alternation of inference and dictionary learning is iterated until a certain convergence criteria is met. Such frameworks have been applied with success to image restoration [20], features extraction [21] and classification [22]. Extensions of these models have been proposed to include convolutional dictionaries [23, 21] and hierarchical structure of the representations [22], leading to a new kind of hierarchical sparse convolutional models. In particular, Sulam et al. proposed a Multi-Layer Convolutional Sparse Coding (ML-CSC) model [24] for unsupervised feature extraction and semi-supervised classification on the MNIST dataset. Interestingly, a parallel has been drawn between the ML-CSC and deep convolutional networks [25].

Sparse coding is also a field of interest for computational neuroscientists. Olshausen & Field [9] first demonstrated that a sparse coding strategy was sufficient to account for the emergence of features similar to the Receptive Fields (RFs) of simple cells in the mammalian primary visual cortex (V1). These RFs are spatially localized, oriented band-pass filters [8]. In neuroscience, sparse coding could also be considered as a result of a competition mechanism that explains sensory input in term of a small number of possible causes (called features in machine learning). In other words, sparse coding implements an 'explaining away' strategy [26]: it suppresses alternative explanations by selecting only the dominant causes. Rao & Ballard [12] were the first to leverage sparse coding strategies into a hierarchical model using the Predictive Coding (PC) framework. Central to the PC theory is the assumption that stimuli are built from a hierarchical generative model. From this perspective, the goal of the PC model consists in solving an inverse problem to find the features (i.e. the causes) of the generative model

that initially created the input stimulus. PC achieves this task through an update scheme that integrates feed-back and feed-forward connections. It consists in minimizing the mismatch between the sensory data (as it propagates through feed-forward connection) and the prediction produced by the expected causes [12] (carried by the feed-back connection). Later, this notion has been generalized into a unified brain theory for perception and action [27]. PC is capable of performing the complex inference required to recognize objects in natural images with a shallow network [26, 13]. PC is also used to predict future frames in a video sequence [28], with each layer of the network making local predictions and only forwarding deviations from those predictions to subsequent layers. However, this model was not able to sufficiently abstract representation to support such tasks as object recognition. Recently, a Predictive Coding Network (PCN) was trained in a supervised manner to recognize objects [29].

The closest models to the proposed one are the PCN [29] and the ML-CSC [24]. On one hand, the PCN from [29] is also fully taking advantage of the bi-directional update scheme of the PC theory. However, the PCN is not including sparsity constraints to the generated representations, and thus has a different inference algorithm. On the contrary, the proposed SDPC network includes a  $\ell_1$ -penalty to each layer that constrains the sparseness of the corresponding representation. Last but not least, the PCN weights are trained using a supervised back-propagation, whereas in the case of SDPC the training is performed without any supervision (unsupervised learning). On the other hand, the ML-CSC [24] is a hierarchical, unsupervised, sparse and convolutional model which shares the most mathematical similarities with our model. Additionally, this model uses the same pursuit algorithms as ours (ISTA and FISTA). However, our network differs from the ML-CSC in two important aspects. First, the ML-CSC encodes only the deepest layer: intermediate layers are not explicitly computed, instead they are implicitly estimated by factorizing a single-layer dictionary (called effective dictionary) into smaller and simpler sparse dictionaries. Consequently, the ML-CSC cannot account for non-linear interactions between layers [30]. On the contrary, the SDPC is explicitly inferring all the sparse representations, allowing us to tune directly the sparseness of the layers. Second, our network computes a bidirectional recurrent process with feed-back and feed-forward interaction between layers.

### 3. The proposed model

In this section, we present the Sparse Deep Predictive Coding (SDPC) model. First, we introduce the notation we use and formalize the mathematical problem addressed by the SDPC. Then, we describe the architecture of the model as well as the mathematics leading to the loss function that needs to be minimized to train the SDPC model. Next, we introduce a gain factor to generalize our model to (very) deep network, and we add the notion of connection strength that allows us to finely tune our model. Finally, we describe some of the core training mechanisms, and we detail the inference algorithm involved in the SDPC.

#### 3.1. Notation and mathematical problem

In our mathematical description of the proposed model, italic letters are used as symbols for *scalars*, bold lowercase letters for column ***vectors*** and bold uppercase letters for **MATRICES**. We assume that our input stimulus  $\mathbf{x}$  is well described by the following hierarchical sparse generative model (Eq. 1):

$$\begin{cases} \mathbf{x} = \mathbf{D}_1^T \boldsymbol{\gamma}_1 + \boldsymbol{\epsilon}_1 & \text{s.t. } \|\boldsymbol{\gamma}_1\|_0 < \alpha_1 \\ \boldsymbol{\gamma}_1 = \mathbf{D}_2^T \boldsymbol{\gamma}_2 + \boldsymbol{\epsilon}_2 & \text{s.t. } \|\boldsymbol{\gamma}_2\|_0 < \alpha_2 \\ .. \\ \boldsymbol{\gamma}_{L-1} = \mathbf{D}_L^T \boldsymbol{\gamma}_L + \boldsymbol{\epsilon}_L & \text{s.t. } \|\boldsymbol{\gamma}_L\|_0 < \alpha_L \end{cases} \quad (1)$$

where  $\boldsymbol{\gamma}_i$  is the sparse representation at layer  $i$  of the input  $\mathbf{x}$  and encoded by the dictionary  $\mathbf{D}_i$ . The sparsity of the representation  $\boldsymbol{\gamma}_i$ , as measured by the number of non-zero coefficients, specified by the  $\ell_0$  pseudo-norm ( $\|\cdot\|_0$ ), is constrained by the scalar  $\alpha_i$ . The number of layers of our model is denoted  $L$  and  $\boldsymbol{\epsilon}_i$  is an additive noise. The core objective of the SDPC model is to retrieve the set of causes (as represented in the dictionaries  $\mathbf{D}_i$ ) that best describes the input  $\mathbf{x}$ . The set of dictionaries  $\{\mathbf{D}_i\}_{i=1}^L$  represents then the learnable parameters of the SDPC, and the sparse representations  $\{\boldsymbol{\gamma}_i\}_{i=1}^L$  are the state variables of the model. Each dictionary has a convolutional structure (i.e. Toeplitz-structured matrices). Thus, we interpret each layer state variable  $\boldsymbol{\gamma}_i$  as a feature map.

#### 3.2. Sparse Deep Predictive Coding (SDPC) architecture

Fig.1 shows the architecture of a 3-layered SDPC model that takes an image  $\mathbf{x}$  as an input. As the SDPC is relying on the Predictive Coding (PC) theory [12], it is continuously generating top-down predictions such that the

representation at one level ( $\gamma_i$ ) predicts the activity of the representation at the lower level ( $\gamma_{i-1}$ ). The prediction from a higher level is sent through a feed-back connection to be compared to the actual representation. This elicits a prediction error,  $\epsilon_i$ , that is forwarded to the following layer to update the representation towards improved prediction. This dynamical process repeats throughout the hierarchy until the bottom-up process no longer conveys any new information to update the corresponding state variable.

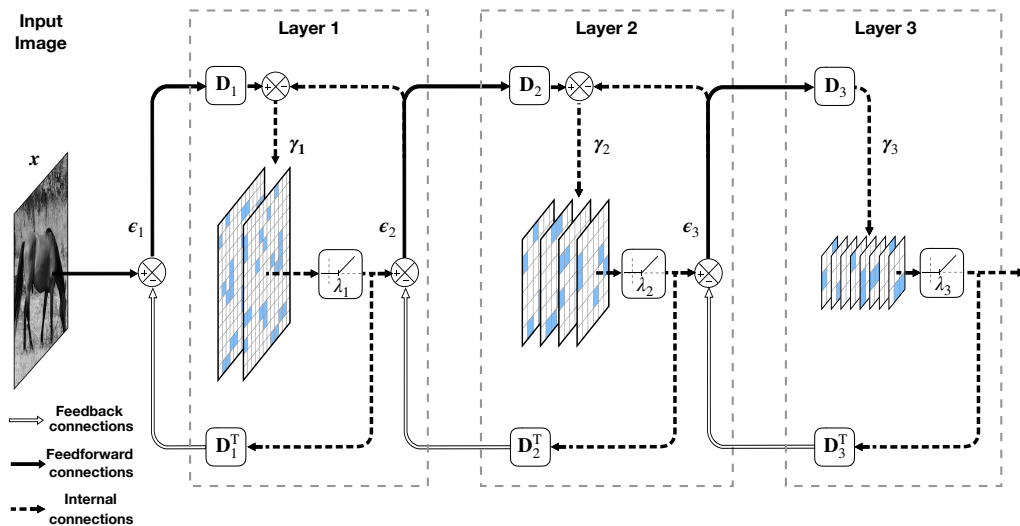


Figure 1: Architecture of a 3-layered SDPC model. In this model  $\gamma_i$  is the layer-specific sparse representation of the image,  $\epsilon_i$  is the representation error (also called prediction error) at layer  $i$ . The synaptic weights of the feed-back and feed-forward connection at each layer ( $\mathbf{D}_i$ ) are reciprocal. Internal representations at layer  $i$  are passed through a non-linearity to force sparseness. The level of sparseness is tuned with the  $\lambda_i$  parameter.

The dictionaries  $\mathbf{D}_i$  could be interpreted as the synaptic weights between the layer  $i - 1$  and the layer  $i$ . We force the weights of the feed-forward connection ( $\mathbf{D}_i$ ) to be reciprocal to the weights of the feed-back connection ( $\mathbf{D}_i^T$ ) [12, 13]. As a consequence, our SDPC model has the same number of parameters than its pure feed-forward equivalent [29]. Interestingly, these dictionaries could be used to project (or back-project) a layer's representation or a dictionary into the next (or previous) layer space. Due to their high dimensionality, the raw dictionaries  $\mathbf{D}_i$  are difficult to interpret and visualize for  $i > 1$  as they represent a structure into an intermediate feature space at

layer  $i - 1$ . To overcome this limitation, we transform the dictionary  $\mathbf{D}_i$  into an effective dictionary  $\mathbf{D}^{(i)}$ , by back-projecting it into the input space, that is in visual space [24]. We call Receptive Fields (RFs) the preferred features of these effective dictionaries. The back-projection mechanism is illustrated in Fig.2.

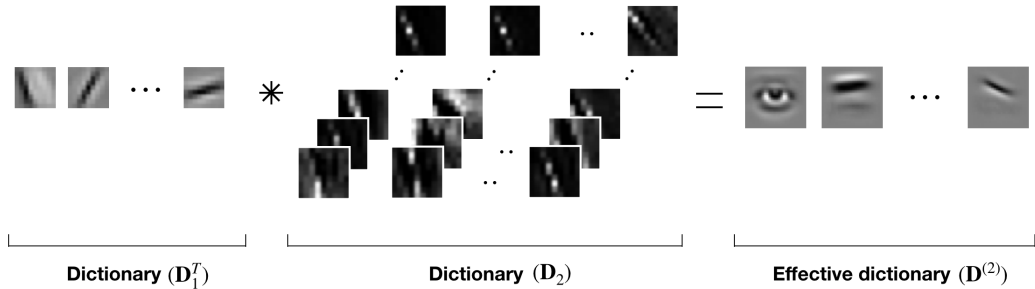


Figure 2: Generation of the second-layer effective dictionary. For the sake of visualization the Toeplitz-structured matrices are viewed as four-dimensional convolutional kernels ([24]). Consequently, we replace the matrix multiplication by a convolutional product.

Differently from the original PC model [12], we enforce in the SDPC a certain level of sparsity by imposing a  $\ell_1$ -penalty to every feature map  $\gamma_i$ . We replaced the layer  $\ell_0$ -regularization used in Eq. 1 by a  $\ell_1$ -regularization, this choice is justified by the fact that the  $\ell_1$ -regularization also induces sparsity, while defining a convex optimization problem. Therefore, we can now use first-order method to solve our mathematical problem. The strength of this  $\ell_1$ -penalty is set by the scalars  $\{\lambda_i\}_{i=1}^L$ . Intuitively,  $\lambda_i$  is tuning the trade-off between the fidelity of  $\mathbf{D}_i^T \gamma_i$  to  $\gamma_{i-1}$  and the sparsity of the representation. A high  $\lambda_i$  will tend to produce a very sparse  $\gamma_i$  and will tend to increase  $\epsilon_i$ . Inversely, lowering  $\lambda_i$  will decrease the level of sparseness of  $\gamma_i$  as well as the prediction error. The  $\ell_1$ -penalty is materialized in Fig.1 by a box containing a non-linearity parameterized by  $\lambda_i$ . The prediction error at layer  $i$ ,  $\epsilon_i$ , is computed as the difference between  $\gamma_{i-1}$  and the back-projection of  $\gamma_i$  into the  $\gamma_{i-1}$  space as shown in Eq. 2:

$$\epsilon_i = \begin{cases} x - \mathbf{D}_1^T \gamma_1 & \text{if } i = 1 \\ \gamma_{i-1} - \mathbf{D}_i^T \gamma_i & \text{if } i \in \llbracket 2; L \rrbracket \end{cases} \quad (2)$$

In the PC model, each state variable  $\gamma_i$  receives two types of influences. One one hand,  $\gamma_i$  is updated to provide a better prediction of the lower-level state variable  $\gamma_{i-1}$ . On the other hand,  $\gamma_i$  is also modified to make sure it is well predicted by the upper-level state variable  $\gamma_{i+1}$ . Therefore, we define the layer-specific loss function,  $\mathcal{L}_i$ , as formulated in Eq. 3:

$$\mathcal{L}_i = \begin{cases} \frac{1}{2}\|\epsilon_i\|_2^2 + \frac{1}{2}\|\epsilon_{i+1}\|_2^2 + \lambda_i\|\gamma_i\|_1 & \text{if } i \in \llbracket 1; L-1 \rrbracket \\ \frac{1}{2}\|\epsilon_L\|_2^2 + \lambda_L\|\gamma_L\|_1 & \text{if } i = L \end{cases} \quad (3)$$

By minimizing the layer loss functions, one can infer the best sparse representations using proximal gradient methods, like ISTA or FISTA [15]. These sparse coding algorithms consist in computing the gradient of  $\mathcal{L}_i$  w.r.t.  $\gamma_i$  and to update the current estimate of  $\gamma_i$  using a proximal operator corresponding to the penalty term. For the  $\ell_1$ -penalty, the optimal proximal operator is the soft-thresholding operator. In addition, we have included a non-negativity constraint on the sparse map. Therefore, we use the element-wise non-negative soft-thresholding operator, denoted  $\mathcal{T}_\alpha$ , as a proximal operator (Eq. 4). Interestingly, in a neuroscience perspective, all the layer state variables  $\gamma_i$  could now be considered as neuronal activity maps where each coefficient of the maps corresponds to the firing rate of the corresponding neuron.

$$\mathcal{T}_\alpha(x) = \begin{cases} x - \alpha & \text{if } x \geq \alpha \\ 0 & \text{if } x \leq \alpha \end{cases} \quad (4)$$

Eq. 5 shows the general update scheme using proximal gradient methods. In this equation  $\eta_{c_i}$  represents the learning rate of the inference step for each layer, it is set to be equal to the inverse of the largest eigenvalue of  $(\mathbf{D}_i^T \mathbf{D}_i)$ . Note that other methods could also be employed to find the optimal  $\eta_{c_i}$  (e.g. line search algorithms like backtracking [15]).

$$\gamma_i \leftarrow \mathcal{T}_{\eta_{c_i}\lambda_i}(\gamma_i - \eta_{c_i} \frac{\partial \mathcal{L}_i}{\partial \gamma_i}) = \begin{cases} \mathcal{T}_{\eta_{c_i}\lambda_i}(\gamma_i + \eta_{c_i} \mathbf{D}_i \epsilon_i - \eta_{c_i} \epsilon_{i+1}) & \text{if } i \in \llbracket 1; L-1 \rrbracket \\ \mathcal{T}_{\eta_{c_L}\lambda_L}(\gamma_L + \eta_{c_L} \mathbf{D}_L \epsilon_L) & \text{if } i = L \end{cases} \quad (5)$$

This update scheme is the core of the Iterative Soft Thresholding Algorithm (ISTA). In the SDPC model, we use a variant of the ISTA: the Fast Iterative Soft Thresholding Algorithm (FISTA). The main difference between those

two algorithms, it that FISTA adds an optimal momentum term in the update scheme that ensures a faster convergence [15]. See Algo. 1 for more details on our FISTA implementation.

### 3.3. Gain factor and upper/lower level strength

When we use the non-negative  $\ell_1$ -penalty as a sparse prior, it is easy to show that we assume *a priori* that the coefficients of the sparse maps follow an exponential probability density function. The direct consequence is that, for a given sparse map, low activation values are more probable. In other words, the non-zero coefficients of a sparse representation will hold very low values. This property, combined with the fact that we are imposing sparser representations for deeper layers leads to a tremendous decrease in activations along the network. This phenomenon is raising two major issues. On one hand, it prevents us from adding as many layers as desired: up to a certain level, activations will be so small that the energy transmitted to the next level will start to be negligible. On the other hand, the amplitude of the loss function (and the gradient) associated with the deepest layers will be so low, that the corresponding inference process will become very inefficient and slow. To overcome this obstacle, we amplify the state variables at layer  $i$  with a constant gain (denoted  $v_i$ ), and we compensate for the amplification of the state variable of the layer  $i + 1$  by dividing the corresponding prediction error by the constant gain  $v_i$ . Therefore, we reformulate the original layer prediction error (Eq. 2) and loss function (Eq. 3) to include the gain factor with Eq. 6 and Eq. 7, respectively.

Decomposing the layer loss function into an upper-level and a lower-level influence (Eq. 3) allows us to tune them separately. In Eq. 7 we denote by  $k_{LL}$  the strength of the lower-level action and by  $k_{UL}$  the impact of the upper-level. Intuitively, if we choose  $k_{LL} < k_{UL}$  we will improve the capability of the deeper layers to explain the activity of the previous layers, consequently more importance will be given to the global structure of the image. Inversely, having  $k_{LL} > k_{UL}$  will prioritize the local structure given by the first layers at the expense of a loss of understanding of the global structure of the input image.

$$\epsilon_i = \begin{cases} \mathbf{x} - \mathbf{D}_1^T \boldsymbol{\gamma}_1 & \text{if } i = 1 \\ v_{i-1} \boldsymbol{\gamma}_{i-1} - \mathbf{D}_i^T \boldsymbol{\gamma}_i & \text{if } i \in [2; L] \end{cases} \quad (6)$$

$$\mathcal{L}_i = \begin{cases} \frac{k_{LL}}{2} \|\boldsymbol{\epsilon}_i\|_2^2 + \frac{k_{UL}}{2v_i^2} \|\boldsymbol{\epsilon}_{i+1}\|_2^2 + \lambda_i \|\boldsymbol{\gamma}_i\|_1 & \text{if } i \in \llbracket 1; L-1 \rrbracket \\ \frac{k_{LL}}{2} \|\boldsymbol{\epsilon}_L\|_2^2 + \lambda_L \|\boldsymbol{\gamma}_L\|_1 & \text{if } i = L \end{cases} \quad (7)$$

### 3.4. Network training

During the inference step, we update the state variables,  $\boldsymbol{\gamma}_i$ , by calculating the gradient of the loss function w.r.t.  $\boldsymbol{\gamma}_i$ , and thus we consider the dictionary  $\mathbf{D}_i$  to be fixed.

**Dictionary learning.** In the dictionary learning step, we do the opposite: we fix  $\boldsymbol{\gamma}_i$  and we update  $\mathbf{D}_i$  using a gradient descent on the corresponding layer loss function. Eq. 8 shows the update rule to learn the dictionaries at each layer,  $\eta_{L_i}$  denotes the step size of the gradient for the layer  $i$ :

$$\forall i \in \llbracket 1; L \rrbracket, \quad \mathbf{D}_i \leftarrow \mathbf{D}_i - \eta_{L_i} \frac{\partial \mathcal{L}_i}{\partial \mathbf{D}_i} = \mathbf{D}_i + \eta_{L_i} \boldsymbol{\gamma}_i^T \boldsymbol{\epsilon}_i \quad (8)$$

Each column of  $\mathbf{D}_i$  is  $\ell_2$ -normalized after the update step to avoid any redundant solution.

**Dictionary initialization.** When the representations are forced to be very sparse, only a few numbers of features are selected by the inference algorithm to describe the entire training set in the first few epochs. Consequently, in subsequent epochs, the previously selected features tend to be reinforced while the rest of the features are not adjusted. This problem might arise from a bad initialization of the dictionaries. It can be addressed by an homeostasis regulation on the activation probability of the features [31], or by scheduling the sparsity of the first epochs [32]. For simplicity, we choose the latter solution. We initialize our dictionary such that during the first epochs the sparsity is lower, to ensure that every atom is selected at the beginning of the training. We start the learning with very low sparsity coefficients  $\{\lambda_i\}_{i=1}^L$ . After few iterations, we increase progressively, or in one shot, each  $\lambda_i$  to its final value. We call initialization epochs the epochs when the sparsity is lower than the targeted one. This heuristic allows us to have all the features selected even when the sparsity level becomes very high.

**Implementation.** We used PyTorch version 0.4.1 [33], leveraged with a GPU (Nvidia GTX 1080 Ti) to implement our SDPC model. The pseudo-code of the inference step is described in Algo. 1. In addition, the full python implementation of the SDPC model and the simulations used to generate the

results will be available, once the article published, at [https://github.com/VictorBoutin/SDPC\\_V0.git](https://github.com/VictorBoutin/SDPC_V0.git).

---

**Algorithm 1:** SDPC inference algorithm

---

**input** : image:  $\mathbf{x}$ , dictionaries:  $\{\mathbf{D}_i\}_{i=1}^L$ ,  $\ell_1$ -penalty parameters:  $\{\lambda_i\}_{i=1}^L$ , gain factors:  $\{v_i\}_{i=1}^{L-1}$ , upper & lower level strength:  $(k_{LL}, k_{UL})$

$\gamma_0 = \mathbf{x}, \{\gamma_i\}_{i=1}^L = \mathbf{0}$  # Initializing layer state variables

$\{\gamma_i^z\}_{i=1}^L = \{\gamma_i^o\}_{i=1}^L = \{\gamma_i\}_{i=1}^L$  # Initializing FISTA momentum

$v_0 = 1, v_L = 1$  # making the algorithm more compact

$\eta_{c_i} = \frac{1}{\max(\text{eigen\_value}(\mathbf{D}_i^T \mathbf{D}_i))}$

$t^o = 1, it = 1$

**while** convergence **do**

$t^n = \frac{1 + \sqrt{1 + 4(t^o)^2}}{2}$

**for**  $i = 1$  **to**  $L$  **do**

# Update lower-layer error

$\epsilon_{LL} = v_{i-1} \gamma_{i-1}^z - \mathbf{D}_i^T \gamma_i^z$

# Update the upper-layer error

**if**  $i \neq L$  **then**

$\epsilon_{UL} = v_i \gamma_i^z - \mathbf{D}_{i+1}^T \gamma_{i+1}^z$

**else**

$\epsilon_{UL} = \mathbf{0}$

# Update layer state variables using FISTA momentum

$\gamma_i = \mathcal{T}_{\eta_{c_i} \lambda_i}(\gamma_i^z + \eta_{c_i} k_{LL} \mathbf{D}_i \epsilon_{LL} - \frac{\eta_{c_i}}{v_i} k_{UL} \epsilon_{UL})$

$\gamma_i^z = \mathcal{T}_0\left(\gamma_i + \left(\frac{t^o - 1}{t^n}\right)(\gamma_i - \gamma_i^o)\right)$

$\gamma_i^o = \gamma_i$

$t^o = t^n, it += 1$

**return**  $\{\gamma_i^z\}_{i=1}^L$

---

**Note:**  $\mathcal{T}_\alpha(\cdot)$  denotes the element-wise non-negative soft-thresholding operator. A fortiori,  $\mathcal{T}_0(\cdot)$  is a rectified linear unit operator. # comments are comments.

## 4. Experiments

In this section, we present the experimental results obtained with the proposed Sparse Deep Predictive Coding (SDPC) model. First, we describe the parameters of the model. Second, we present the features extracted on a database of face images and draw a parallel of this modeling result with neuroscience. Third, we analyze the results of a similar experiment conducted on a standard Machine Learning dataset and perform additional classification experiments to assess the efficiency of the representation at the output of our model.

### 4.1. Experimental Settings

**Datasets.** We train our SDPC model to extract features on two different datasets: the AT&T face database [34], and a dataset of handwritten digits, MNIST [35]. Indeed, we chose to use the AT&T database as face images allow for the qualitative assessment of the meaningfulness of extracted features. Moreover, as neuroscientists have conducted many experiments using face databases, this allows us to draw an interesting parallel with biological recordings. Note that one drawback of the AT&T database is that it has not enough images per category (10 images per category) to quantitatively assess the features obtained through a classification experiment. For this purpose, the MNIST dataset is chosen as it is the *de facto* benchmark for DL and allows for a quantitative comparison, in particular with the ML-CSC model [24]. On one hand, the AT&T dataset is made with 400 grayscale images of size  $92 \times 112$  pixels (px) representing faces of 40 distinct subjects with different lighting conditions, facial expressions, and details. This set is partitioned into 20 batches. On the other hand, the MNIST database is composed of  $28 \times 28$  px grayscale images representing handwritten digits. The MNIST dataset is split into two different sets: a training set with 60000 images partitioned into 600 batches, and a testing set composed of 10000 images divided into 10 batches. Both databases are pre-processed using Local Contrast Normalization (LCN) [36] to reduce dependency between pixels in the image. LCN has a similar effect on images as the pre-processing stage in the original sparse coding study [9] and is inspired from computational neuroscience [37]. It consists of a local subtractive and divisive normalization (see Fig. 4a for an example of pre-processed images on AT&T). These two databases are randomly shuffled at the beginning of each training epoch.

**Network architecture and training parameters.** For each of the two databases we use the same SDPC model, but with a different network structure and different training parameters. Both sets of parameters are summarized in Table 1.

The SDPC model applied on AT&T is composed of two convolutional layers. We train our model on 50 epochs. Before this training, we initialize the dictionaries by scheduling the layer sparsity parameters during 6 initialization epochs. It allows us to address the “dead units” problem described above. For the first two initialization epochs  $\lambda_i$  is set to 0.05, then to 0.1 for the following two epochs, and to 0.2 for the last two epochs. During the training  $\lambda_1$  is fixed to 0.5 and  $\lambda_2$  to 1.

The SDPC model trained on MNIST is composed of 3 convolutional layers. We also initialized our dictionaries by scheduling the sparsity parameters during 6 initialization epochs.  $\lambda_1$ ,  $\lambda_2$ ,  $\lambda_3$  are set respectively to 0.02, 0.02, 0.005 in the 2 first initialization epochs, then 0.02, 0.02, 0.01 in the following 2 initialization epochs, and finally 0.02, 0.02, 0.02 for the 2 last initialization epochs. During the training,  $\lambda_1$  is fixed to 0.09,  $\lambda_2$  to 0.06, and  $\lambda_3$  to 0.06.

#### 4.2. SDPC on AT&T database

Fig. 3 shows the evolution of the global loss (Fig. 3a) and the sparsity (Fig. 3b) of each layer during the training on the AT&T database. The global loss corresponds to the sum of all the prediction errors with respect to each layer: i.e.  $\sum_{i=1}^L \|\epsilon_i\|_2^2$ . At the end of the training, we observed that the loss and all the layer’s sparsity have converged to a stable point. The first-layer feature map reaches a sparsity of 92.85%, meaning that approximately 10000 coefficients are used to encode the input image in this layer. Concerning the second-layer state variable, it is 99.41% sparse, in other words, approximately 1120 coefficients are activated to represent the input in the deepest layer.

Fig. 4 presents the RFs and the reconstruction for each layer once the model is trained on the AT&T database. Appendix A refers to a video of the evolution of the RFs during the training. We remind that we call RFs, the features of the effective dictionaries. These RFs could be compared with the notion of “preferred” stimulus used in electrophysiology, that is, for any given neuron the visual stimulus that produces the strongest activity. The first-layer RFs (Fig. 4b) are spatially localized, oriented, and band-pass filtered as observed in biology [8] and in shallow models [9].

The representation of the second-layer RFs (Fig. 4d) are built from a linear combination of the first-layer RFs. In general, these RFs exhibit more

	param. symbol	SDPC on AT&T	SDPC on MNIST
network param.	$[\mathbf{D}_1 \text{ size}]$ (stride)	[64, 1, 9, 9] (2)	[32, 1, 7, 7] (2)
	$[\mathbf{D}_2 \text{ size}]$ (stride)	[128, 64, 9, 9] (1)	[128, 32, 5, 5] (1)
	$[\mathbf{D}_3 \text{ size}]$ (stride)		[1024, 128, 7, 7] (1)
	$\lambda_1$	0.5	0.09
	$\lambda_2$	1	0.06
	$\lambda_3$		0.06
	$v_1$	1	2
	$v_2$		4
	$k_{LL}$	1	1
training param.	$k_{UL}$	1	8
	$\eta_{L_1}$	$1.5 \times 10^{-3}$	$5 \times 10^{-2}$
	$\eta_{L_2}$	$5 \times 10^{-1}$	$1 \times 10^{-1}$
	$\eta_{L_3}$		$5 \times 10^{-1}$
number of epochs		50	20
sparse map properties	$[\gamma_1 \text{ size}]$	[64, 52, 42]	[16, 11, 11]
	$[\gamma_2 \text{ size}]$	[128, 44, 34]	[128, 7, 7]
	$[\gamma_3 \text{ size}]$		[1024, 1, 1]
	$\ \gamma_1\ _0$ (% level)	$\approx 10000$ (92.85%)	$\approx 551$ (71.52%)
	$\ \gamma_2\ _0$ (% level)	$\approx 1120$ (99.41%)	$\approx 699$ (88.84%)
	$\ \gamma_3\ _0$ (% level)		$\approx 33$ (96.70%)

Table 1: Parameters of SDPC models applied on AT&T and MNIST. The dictionary size is shown in the format: [number of features, number of channels, width, height] (value of the convolutional stride). The size of the sparse map is shown in the format: [number of maps, width, height]. The sparsity level in percentage corresponds to the  $\ell_0$  pseudo-norm divided by the volume of the sparse map. Cells left blank for the AT&T model, corresponds to third-layer parameters, and thus are not applicable to a 2-layers model.

complex, and less generic filters such as long lines and curvatures. In particular, we observe the emergence of highly face-specific features such as eyes, noses or eyebrows. When comparing the input image (Fig. 4a) with the first-layer prediction (Fig. 4c), we observe that the latter is slightly smoothing the textural details (like hairs, skin or beard) and highlighting the contour of the face, the eyes, and the nose. This effect is even more pronounced in the prediction made by the second layer (Fig. 4e): it mainly encodes the shape of the faces and fades most of the textures. Nevertheless, it is still possible to identify the subject behind the face. Only 1% of the coefficients are active

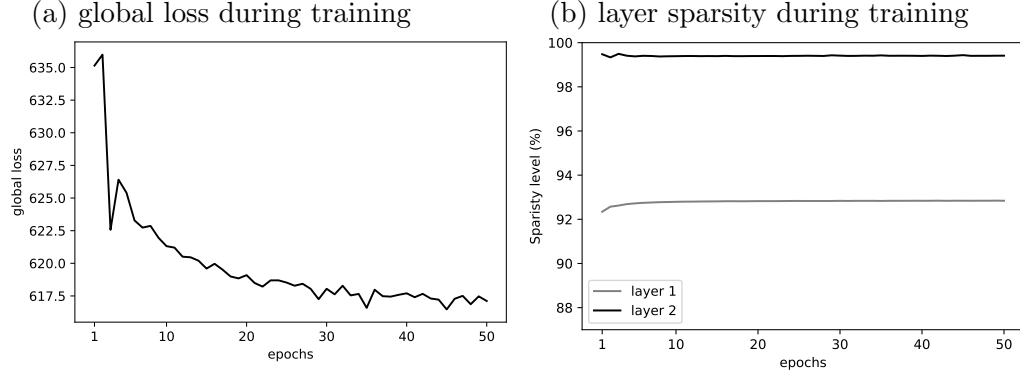


Figure 3: Sparsity and loss evolution during the training on the AT&T database. (a) Evolution of the global loss during the unsupervised learning. The global loss is computed as the sum of all the prediction errors defined in Eq. 6. (b) Evolution of the sparsity during the unsupervised learning. The sparsity level at convergence is 92.85% for the first layer and 99.41% for the second layer.

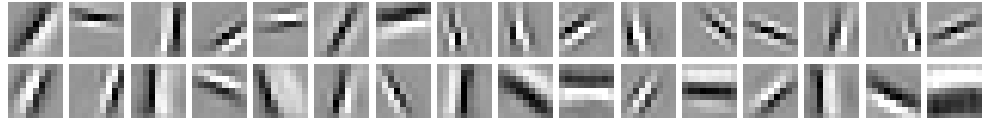
in  $\gamma_2$ , meaning that despite the tremendous loss of information, the SDPC is still able to reconstruct recognizable faces. We notice also some defects in the last-layer prediction: the last 3 images of Fig. 4e show worst-case examples which exhibit poorly encoded eyes and nose. Given the relatively high resolution of the second-layer RFs, specific face features (e.g. eyes and nose) hold a high range of variability, being highly pose and subject dependent. Consequently, the model tends to learn an average feature rather than adapting to specific ones. In this example, the responses to the input at these particular locations are weaker when eyes and nose are poorly encoded by the corresponding features learned by the SDPC. On the contrary, glasses (5th image of Fig. 4e) and wrinkles (6th image of Fig. 4e) are easily explained, at this scale, by general filters such as lines and oriented Gabor-filters. One solution to fix this problem would be to induce some invariance to translation and elastic transformations by introducing a spatial pooling on the network activity. As a result, we believe that this would increase the generalization power of SDPC.

Working with natural images, and especially with a face database, allows us to draw a parallel with computational and experimental neuroscience. Interestingly, the first-layer RFs (Fig. 4b) are similar to the preferred stimuli of V1 simple-cells, which are oriented Gabor-like filters [8]. Therefore, our

(a) Examples of AT&T images after pre-processing



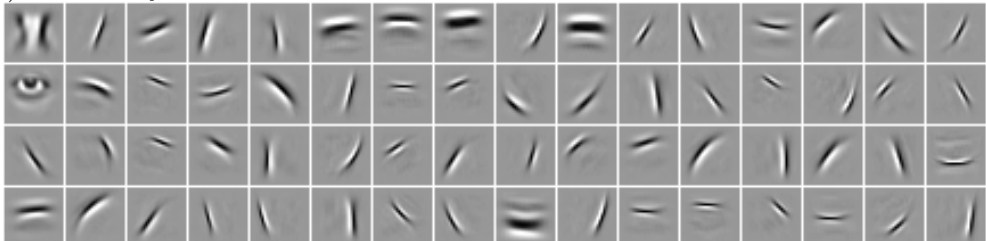
(b) First-layer RFs



(c) First-layer reconstruction



(d) Second-layer RFs



(e) Second-layer reconstruction



Figure 4: Input, features and reconstructed input after the training on the AT&T database. (a) Images pre-processed with Local Contrast Normalization [36]. (b) 32 randomly selected first-layer RFs from  $\mathcal{D}^{(1)}$ . (c) First-layer reconstruction, generated by back-projecting  $\gamma_1$  into the input space. (d) 64 second-layer RFs (randomly selected) of size  $28 \times 28$  px, drawn from the effective dictionary  $\mathcal{D}^{(2)}$ . (e) Second-layer reconstruction, generated by back-projecting  $\gamma_2$  into the input space, showing 3 best examples (left) and the 3 worst.

SDPC model is fully in line with the theory stating that such filters emerged from sparse coding strategies [9]. In addition, neurons found in macaque infero-temporal cortex (one of the highest area of the ventral visual pathway) are known to be object-specific [38] whereas those located in the first areas of the visual cortex (V1, V2) have more generic preferred stimuli. This increase in specificity and in the level of abstraction when going deeper in the hierarchies of the network is also one of the results emerging from the proposed model. In particular, we found that the second-layer RFs (Fig. 4c) are specific to some sub-regions of faces, as it is also shown experimentally in human recordings [39, 40]. Even though the presented results are coherent with biological perception, this is not enough to claim that such a model could be implemented by the brain. To be biologically plausible, a computational model needs to satisfy the following two constraints: local computation and local plasticity [41]. The locality of the computation is ensured by Eq. 5: the new state of a neuronal population (whose activity is represented by the sparse map  $\gamma_i$ ) only depends on its previous state, its inputs ( $\epsilon_{i+1}$  and  $\epsilon_i$ ) and the associated synaptic weight ( $D_i$ ). Similarly, the update of the synaptic plasticity ( $D_i$ ), described by Eq. 8, is exclusively based on the pre-synaptic and post-synaptic activity ( $\epsilon_{i+1}$  and  $\gamma_i$ , respectively). All these observations reinforce the biological plausibility of the proposed model both in term of processing and results.

The SDPC model is built to solve the hierarchical generative model presented in Eq. 1. Fig. 5 shows an illustration of this model, and gives a meaningful signification of the dictionaries and the layer state variables. The SDPC model, in its deeper layer, represents a face as the sum of various causes (described by the second-layer dictionary  $D_2$ ) located at key positions (depicted by the state variable  $\gamma_2$ ). Interestingly, the combination of the features with their position, in the context of the hierarchical generative model, gives a relevant interpretation of the SDPC decision-making process. It identifies a face as a sum of crucial properties: two symmetrical eyes, one nose in the center, eyebrows over the eyes, a specific contour shape, etc. Similarly, the eyes are viewed by the SDPC as the sum of smaller Gabor-filters with different orientation positioned in a specific manner. Therefore, the generative model has built the abstract idea of eyes from small oriented lines to describe a face. This strategy can be extended to any input that could be explained with a hierarchical generative model.

In this subsection, we have shown that the features learned by the SDPC are general in the first-layers and specific in the deeper-layers. We have

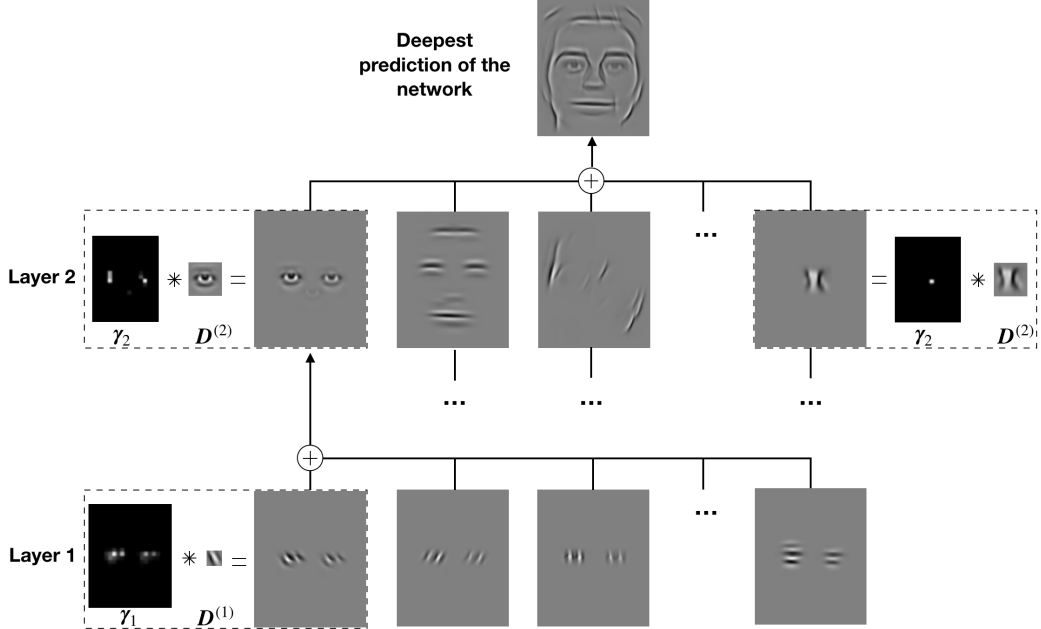


Figure 5: Illustration of the hierarchical generative model learned by the SDPC model on the AT&T database. The deepest prediction (first row) is viewed as the sum of the features prediction (the second row). These feature predictions are computed as the convolution between one channel of  $\gamma_2$  and the corresponding features in  $D_2$ . Similarly, the eyes can be decomposed using  $\gamma_1$  and  $D_1$  (the third row)

demonstrated that the SDPC is biologically plausible. When the features are replaced in the context of the hierarchical generative model, an image could be viewed as the sum of maps conveying relevant and meaningful information.

#### 4.3. SDPC on MNIST Database

Fig. 6 shows the evolution of the total (Fig. 6a) loss and the sparsity (Fig. 6b) of all the layers of the SDPC model on the MNIST dataset. After 20 epochs, the total loss of the model has converged. At the end of the training, the first layer reaches a sparsity level of 71.52% (551 active elements), the second layer is 88.84% sparse (699 active elements) and the last layer is 96.70% sparse (33 active elements).

Fig. 7 shows the RFs of each SDPC-layer trained on the MNIST database. Appendix B refers to a video of the evolution of the RFs during the training.

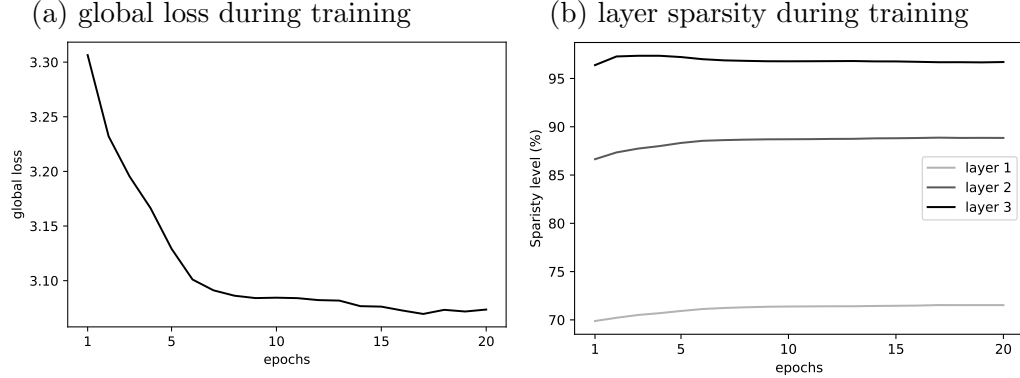
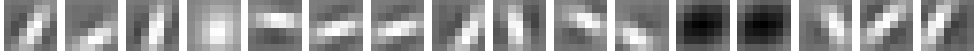


Figure 6: Sparsity and loss evolution during the training on the MNIST database. (a) Evolution of the global loss during the unsupervised training. The global sum is computed as the sum of all the prediction errors defined in Eq. 6. Eq. 7. (b) Evolution of the layer sparsity. The sparsity level at convergence is 71.52%, 88.84% and 96.70% for the first, second and third layer, respectively.

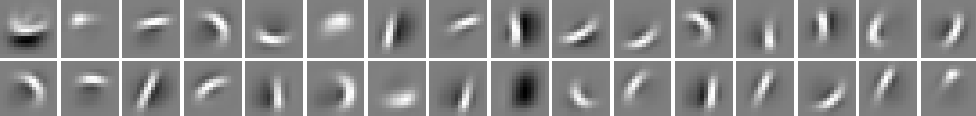
Similarly to the previous experiment conducted on the AT&T database, we observe that the first-layer RFs are small-dimensional edges spanning different orientations. In addition, we note the apparition of very low-frequency filters (the black or white blobs). Deeper-layers RFs follow a higher order statistic and are more specific to the presented image. At first sight, the complexity and the degree of abstraction of the features extracted by the third layer are not higher than those extracted by the second layer. This property is inherent to the very specific network architecture we have used for this experiment. As shown in Table 1, the deepest sparse map of this network has the shape of a vector. Consequently, the last-layer RFs (or the features of the effective dictionary denoted  $\mathbf{D}^{(3)}$ ) have exactly the same size than the whole input image. Therefore, the last-layer sparse map is not encoding anymore for the position of the features, but only for its presence. In other words, the position becomes encoded in the address of the atom itself. This property explains why the second-layer features are well centered in the RFs whereas the features of  $\mathbf{D}^{(3)}$  are very localized. Here also, we observe that the last-layer features are capturing the inherent properties of the MNIST digits. The latter are described in a manner that seems natural and relevant: as a sum of localized loops and strokes.

We compare the features extracted by the SDPC with those learned by the

(a) SDPC first-layer RFs on MNIST



(b) SDPC second-layer RFs on MNIST



(c) SDPC third-layer RFs on MNIST

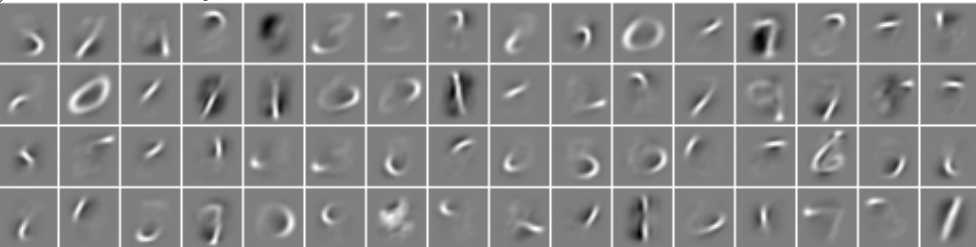


Figure 7: Features extracted by the SDPC after unsupervised training on MNIST. (a) 16 second-layer RFs (randomly selected) of size  $7 \times 7$  pixels, drawn from the effective dictionary  $\mathbf{D}^{(1)}$ . (b) 32 second-layer RFs (randomly selected) of size  $16 \times 16$  pixels, drawn from the effective dictionary  $\mathbf{D}^{(2)}$ . (c) 64 second-layer RFs (randomly selected) of size  $28 \times 28$  pixels, drawn from the effective dictionary  $\mathbf{D}^{(3)}$ .

Multi-Layer Convolutional Sparse Coding (ML-CSC) [24]. Mathematically speaking, those two models are relatively similar, but important architectural differences separate them (Fig. 1 versus Fig. C.1): the ML-CSC performs a global processing on all layers at once, whereas the SDPC is doing only local computations. For comparison purposes, we trained the two models on the same network sizes, and using equivalent sparsity constraints. By comparing the RFs on Fig. 7 and Fig. D.1 we observe that the ML-CSC features are less smooth and more noisy than those obtained with the proposed SDPC model. Moreover, despite the fact that the sparsity in the last layer is the same for both models, we notice that the ML-CSC features are describing a smaller part of the complete digit. The features obtained with the latter model seem to be less relevant, and less meaningful to describe a digit.

Finally, we conducted a classification experiment to assess if the representation of the MNIST digits generated by the SDPC model allows us to identify each digit’s class (the value it represents). For this purpose, we fed a linear classifier with the deepest feature map obtained with the SDPC. The

classifier is trained independently in a supervised manner, using the MNIST labels, whereas the SDPC feature extractor is fully unsupervised. The classifier is composed of two fully-connected layers (size:  $1024 \times 10$ ), with a softmax activation function. The training was performed in 60 epochs using a standard Adam [42] algorithm with a cross-entropy loss function. The learning rate of the Adam optimizer is  $1.10^{-3}$  and the exponential decay rates  $\beta_1$  and  $\beta_2$  are set to 0.9 and 0.999 respectively. We compare, through this classification experiment, the accuracy obtained with the SDPC and ML-CSC features.

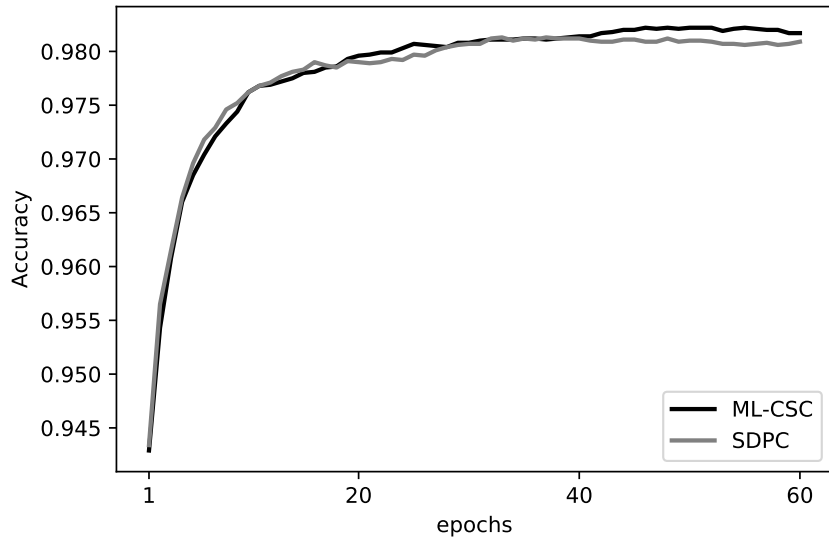


Figure 8: Evolution of the classification accuracy on MNIST during the training of the classifier for the ML-CSC and SDPC models. The accuracy is evaluated on the testing dataset.

Fig. 8 shows the evolution of the classification accuracy on the MNIST testing set during the training of the classifier. We observe that both models produce sparse representations that, once fed into a linear classifier, allows class recognition with an accuracy over 98% (98.12% for ML-CSC and 98.06% for the SDPC). Interestingly enough, while one might think that the global computation performed by the ML-CSC should provide better classification accuracy, this is actually not the case. Our classification experiment proves that the direct knowledge of the input image is not necessary to provide easily classifiable representation. An efficient local processing that conveys

the most informative part of the input is enough to deduce good classification accuracy.

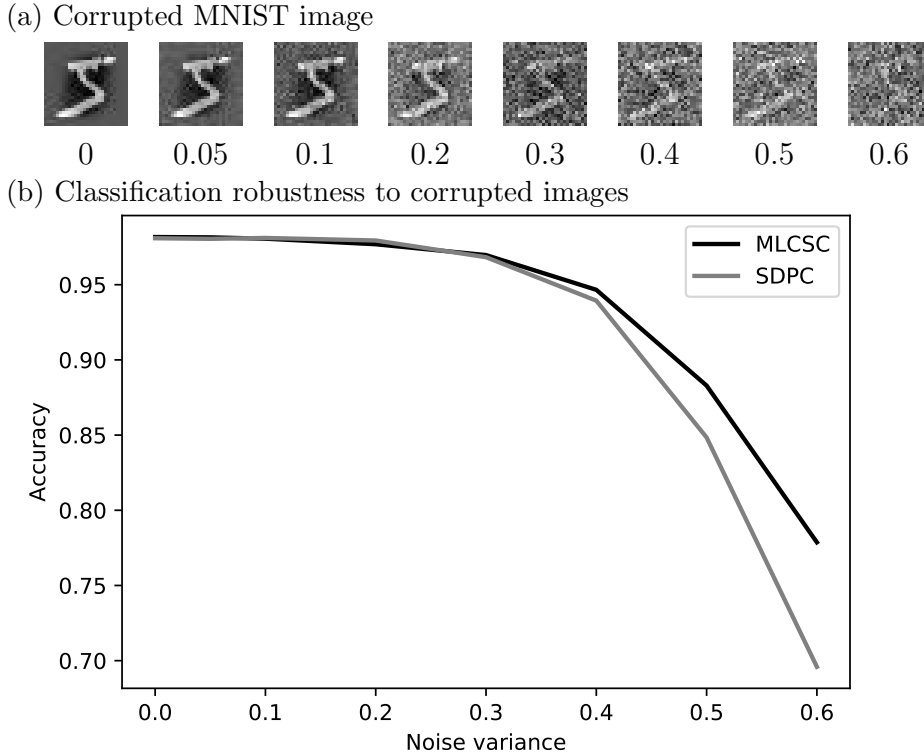


Figure 9: Robustness of the classification accuracy. (a) Examples of noisy MNIST images obtain by adding a gaussian noise with different variance. (b) Testing classification accuracy with corrupted input, for the ML-CSC and the SDPC models.

As a last experiment, we assess the classification robustness of the two models when the input was corrupted with noise. To do so, we add random values to each pixel of the input image, these values are taken from a normal distribution with a mean equal to zero and a variance varying between 0 to 0.6. An example of the corrupted input could be seen on Fig. 9a. The objective of this experiment is to assess how these two models are, by construction, resilient to noisy input. Consequently, we did not train our SDPC model with noisy input images. The training procedure is exactly similar to the one used in the feature extraction experiment. The only difference, is that instead of evaluating the classification accuracy with the standard MNIST testing set, we degraded this set with different levels of noise. Fig. 9b shows the clas-

sification accuracy obtained for both models, and for different perturbation magnitudes (generated by changing the variance of the noise). We observe that the classification accuracy of both models is comparable when the variance of the perturbation is kept under  $\approx 0.4$ . Nevertheless, when the input is highly degraded, the ML-CSC has a higher classification accuracy than the SDPC. For a variance of  $\approx 0.6$ , a human can hardly recognize the digit, but the ML-CSC and the SDPC can classify the noisy MNIST digit with 77% and 70% accuracy, respectively. This results is remarkable if replaced in its context. The ML-CSC model was designed by [24] to theoretically guarantee the recovery and stability of the representations when the input was facing small perturbations. On the contrary, the SDPC model is built on a computational neuroscience framework that has *a priori* no theoretical guarantee concerning the global stability of the representation as all operations are local. Therefore it is surprising how well the local computation of the SDPC model is competing with the global processing of the ML-CSC in term of robustness to classification accuracy.

To sum up, we have confirmed in this subsection that the SDPC model is able to extract meaningful features on the MNIST dataset. In addition, we have shown that these features encode a higher-level representation of the input image that is efficiently classifiable and robust to noisy perturbations.

## 5. Conclusion

In this paper, we have presented a novel model called Sparse Deep Predictive Coding (SDPC) inspired from the powerful computational neuroscience theory of predictive coding. Extending from the characteristics of a multi-layer CNN, we have integrated the predictive coding framework into a sparse hierarchical convolutional model. To the best of our knowledge, this is the first time these properties are combined at the same time within a predictive coding framework. Unlike most of the CNNs, the SDPC has feed-back and feed-forward connections, and then perform a recurrent update scheme to compute its state variables. Interestingly, our model inherits the local processing and plasticity principles that are prerequisites to any computational theory to be implemented by the brain. Moreover, worthwhile parallels could be drawn with results observed in neuroscience. We conduct an experimental analysis of our SDPC model on two image datasets: AT&T and MNIST. The main findings of the paper can be summarized as follows :

- The features extracted by the SDPC are qualitatively similar to those observed in the hierarchy of the mammalian visual cortex: first-layer features are general, and deeper-layer features are more abstract and specific to the type of input stimulus (faces versus digits).
- The features extracted by the SDPC represent the most informative part of the input. These features are crucial to describe the input in a general manner.
- The decision-making process can be visualized by replacing the extracted features in the context of the hierarchical generative model. Indeed, any specific prediction could be explained as a combination of features with their corresponding position (as defined in the feature map).
- The extracted features encode the input image into a representation that is easily classifiable on the MNIST dataset despite the local processing of the SDPC.
- The proposed SDPC can compete with the state-of-the-art model when it comes to classify noisy MNIST images. We show that the SDPC can still recognize MNIST digits even when the latter is so corrupted that its hardly recognizable by a human being.

These results confirm our intention which was to show that by combining biological principles to artificial intelligence, we can better grasp the decision-making process that leads algorithms to a specific prediction. Conversely, we also think that such results may also help better understand computational principles in neuroscience.

We foresee future works to strengthen our results, and first by generalizing our results on more complex and challenging databases. In addition, the SDPC model gives us the flexibility to easily include non-linear functions that modulate the activity of the state variable. Therefore, extensive studies should be conducted to investigate the use of non-linear functions like max-pooling as they show great success in the deep-learning algorithms. Interestingly, it is really easy to transform the SDPC into a fully-supervised model: one need only to include a supervised signal in the loss of the last layer. This will give a framework to compare rigorously the impact of the supervision on the features, on the loss, or on the classification accuracy. Last

but not least, the locality of the processing could be exploited in distributing the layer computation into different parts of a dedicated hardware, such as neuromorphic computing devices. This may drastically speed-up the SDPC to reach real-time capabilities, allowing it for applications like robotics. In particular, the inherent noise-resilience of the SDPC makes it a perfect candidate to perform image-processing in noisy images, like those captured by rotary-wings UAV or in dim-light environment.

## Acknowledgments

We thank M. Elad and J. Sulam for sharing the Matlab code of their ML-CSC frameworks. This project has received funding from the European Union’s Horizon 2020 research and innovation programme under the Marie Skłodowska-Curie grant agreement n°713750. Also, it has been carried out with the financial support of the Regional Council of Provence-Alpes-Côte d’Azur and with the financial support of the A\*MIDEX (n°ANR-11-IDEX-0001-02). This work was granted access to the HPC resources of Aix-Marseille Université financed by the project EquipMeso (ANR-10-EQPX-29-01) of the program ”Investissements d’Avenir”.

## References

- [1] Y. LeCun, Y. Bengio, G. Hinton, Deep learning, *Nature* 521 (2015) 436.
- [2] D. E. Rumelhart, G. E. Hinton, R. J. Williams, Learning representations by back-propagating errors, *Nature* 323 (1986) 533.
- [3] S. Rifai, P. Vincent, X. Muller, X. Glorot, Y. Bengio, Contractive auto-encoders: Explicit invariance during feature extraction, in: Proceedings of the 28th International Conference on International Conference on Machine Learning, Omnipress, pp. 833–840.
- [4] A. Krizhevsky, I. Sutskever, G. E. Hinton, Imagenet classification with deep convolutional neural networks, in: Advances in neural information processing systems, pp. 1097–1105.
- [5] S. Ren, K. He, R. Girshick, J. Sun, Faster r-cnn: Towards real-time object detection with region proposal networks, in: Advances in neural information processing systems, pp. 91–99.
- [6] Y. Hu, A. Soltoggio, R. Lock, S. Carter, A fully convolutional two-stream fusion network for interactive image segmentation, *Neural Networks* 109 (2019) 31–42.
- [7] M. D. Zeiler, R. Fergus, Visualizing and understanding convolutional networks, in: European conference on computer vision, Springer, pp. 818–833.
- [8] D. H. Hubel, T. N. Wiesel, Receptive fields and functional architecture of monkey striate cortex, *The Journal of physiology* 195 (1968) 215–243.
- [9] B. A. Olshausen, D. J. Field, Sparse coding with an overcomplete basis set: A strategy employed by v1?, *Vision research* 37 (1997) 3311–3325.
- [10] D. L. Ringach, Spatial structure and symmetry of simple-cell receptive fields in macaque primary visual cortex, *Journal of neurophysiology* 88 (2002) 455–463.
- [11] M. Elad, Sparse and Redundant Representations: From Theory to Applications in Signal and Image Processing, Springer, New York, 2010 edition edition, 2010. 00000.

- [12] R. P. Rao, D. H. Ballard, Predictive coding in the visual cortex: a functional interpretation of some extra-classical receptive-field effects, *Nature neuroscience* 2 (1999) 79.
- [13] M. W. Spratling, A hierarchical predictive coding model of object recognition in natural images, *Cognitive computation* 9 (2017) 151–167.
- [14] D. C. Knill, A. Pouget, The bayesian brain: the role of uncertainty in neural coding and computation 27 (2004) 712–719.
- [15] A. Beck, M. Teboulle, A fast iterative shrinkage-thresholding algorithm for linear inverse problems, *SIAM journal on imaging sciences* 2 (2009) 183–202.
- [16] S. Mallat, Z. Zhang, Matching pursuit with time-frequency dictionaries, Technical Report, Courant Institute of Mathematical Sciences New York United States, 1993.
- [17] Y. Li, S. Osher, Coordinate descent optimization for  $l_1$  minimization with application to compressed sensing; a greedy algorithm, *Inverse Problems and Imaging* 3 (2009) 487–503.
- [18] R. Rubinstein, A. M. Bruckstein, M. Elad, Dictionaries for sparse representation modeling, *Proceedings of the IEEE* 98 (2010) 1045–1057.
- [19] K. Kreutz-Delgado, J. F. Murray, B. D. Rao, K. Engan, T.-W. Lee, T. J. Sejnowski, Dictionary learning algorithms for sparse representation, *Neural computation* 15 (2003) 349–396.
- [20] J. Mairal, F. Bach, J. Ponce, G. Sapiro, A. Zisserman, Non-local sparse models for image restoration, in: *Computer Vision, 2009 IEEE 12th International Conference on*, IEEE, pp. 2272–2279.
- [21] A. Szelam, K. Kavukcuoglu, Y. LeCun, Convolutional matching pursuit and dictionary training, *arXiv preprint arXiv:1010.0422* (2010).
- [22] L. Bo, X. Ren, D. Fox, Hierarchical matching pursuit for image classification: Architecture and fast algorithms, in: *Advances in neural information processing systems*, pp. 2115–2123.

- [23] R. Chalasani, J. C. Principe, N. Ramakrishnan, A fast proximal method for convolutional sparse coding, in: Neural Networks (IJCNN), The 2013 International Joint Conference on, IEEE, pp. 1–5.
- [24] J. Sulam, V. Petyan, Y. Romano, M. Elad, Multi-layer convolutional sparse modeling: Pursuit and dictionary learning, CoRR abs/1708.08705 (2017).
- [25] V. Petyan, Y. Romano, M. Elad, Convolutional neural networks analyzed via convolutional sparse coding, arXiv preprint arXiv:1607.08194 (2016).
- [26] M. W. Spratling, Unsupervised learning of generative and discriminative weights encoding elementary image components in a predictive coding model of cortical function, *Neural computation* 24 (2012) 60–103.
- [27] K. Friston, Hierarchical models in the brain, *PLoS computational biology* 4 (2008) e1000211.
- [28] W. Lotter, G. Kreiman, D. Cox, Deep predictive coding networks for video prediction and unsupervised learning, arXiv preprint arXiv:1605.08104 (2016).
- [29] H. Wen, K. Han, J. Shi, Y. Zhang, E. Culurciello, Z. Liu, Deep predictive coding network for object recognition, arXiv preprint arXiv:1802.04762 (2018).
- [30] A. Aberdam, J. Sulam, M. Elad, Multi layer sparse coding: the holistic way, arXiv preprint arXiv:1804.09788 (2018).
- [31] L. U. Perrinet, Role of homeostasis in learning sparse representations., *Neural computation* 22 (2010) 1812–36.
- [32] A. Makhzani, B. Frey, K-sparse autoencoders, arXiv preprint arXiv:1312.5663 (2013).
- [33] A. Paszke, S. Gross, S. Chintala, G. Chanan, E. Yang, Z. DeVito, Z. Lin, A. Desmaison, L. Antiga, A. Lerer, Automatic differentiation in pytorch, NIPS 2017 Workshop (2017).
- [34] ATT, Face Database, AT&T Laboratories, Cambridge, 1994.

- [35] Y. LeCun, The MNIST database of handwritten digits, <http://yann.lecun.com/exdb/mnist/> (1998).
- [36] K. Jarrett, K. Kavukcuoglu, Y. LeCun, et al., What is the best multi-stage architecture for object recognition?, in: Computer Vision, 2009 IEEE 12th International Conference on, IEEE, pp. 2146–2153.
- [37] S. Lyu, E. P. Simoncelli, Nonlinear image representation using divisive normalization, in: Computer Vision and Pattern Recognition, 2008. CVPR 2008. IEEE Conference on, IEEE, pp. 1–8.
- [38] C. Bruce, R. Desimone, C. G. Gross, Visual properties of neurons in a polysensory area in superior temporal sulcus of the macaque., *Journal of neurophysiology* 46 (1981) 369–384.
- [39] L. Henriksson, M. Mur, N. Kriegeskorte, Faciotopy—a face-feature map with face-like topology in the human occipital face area, *Cortex* 72 (2015) 156–167.
- [40] H. Leder, C.-C. Carbon, Part-to-whole effects and configural processing in faces, *Psychology Science* 46 (2004) 531–543.
- [41] J. C. Whittington, R. Bogacz, An approximation of the error backpropagation algorithm in a predictive coding network with local hebbian synaptic plasticity, *Neural computation* 29 (2017) 1229–1262.
- [42] D. P. Kingma, J. Ba, Adam: A method for stochastic optimization, arXiv preprint arXiv:1412.6980 (2014).

## **Appendix A. Evolution of the SDPC features during the training on the AT&T database**

A video of the evolution of each layers' RFs during the 50 epochs of the training on the AT&T database could be found at: <https://youtu.be/0CFrmgEcGpw>. The beginning of the video shows the initialization epochs, with the corresponding sparsity written in red. Then the training epochs, and the sparsity are displayed in green

## **Appendix B. Evolution of the SDPC features during the training on the MNIST database**

A video of the evolution of each layers' RFs during the 20 epochs of the training on the MNIST database could be found at : [https://youtu.be/br\\_htrHoCCU](https://youtu.be/br_htrHoCCU). The beginning of the video shows the initialization epochs, with the corresponding sparsity written in red. Then the training epochs, and the sparsity are displayed in green

## Appendix C. Processing architecture of the ML-CSC.

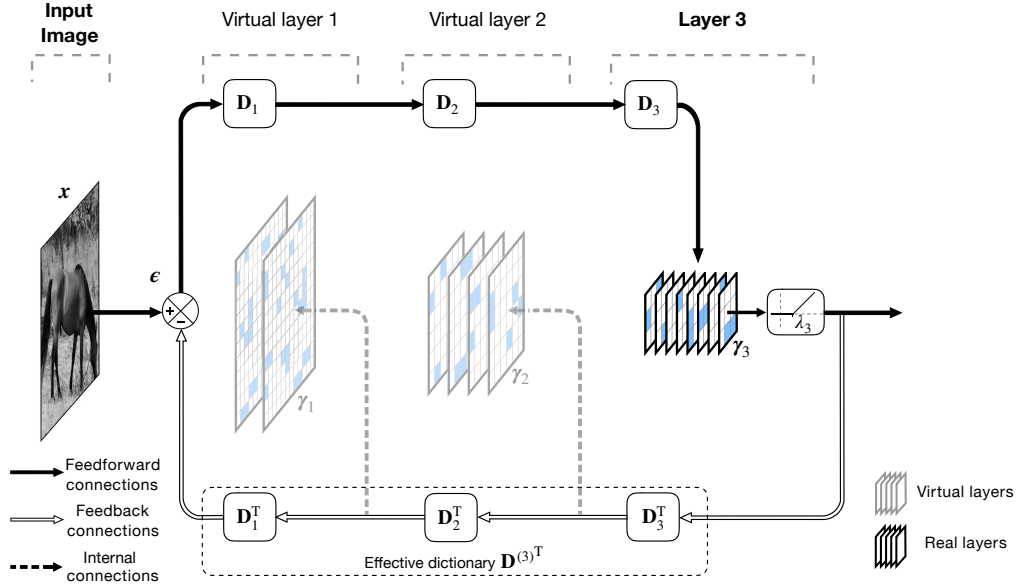


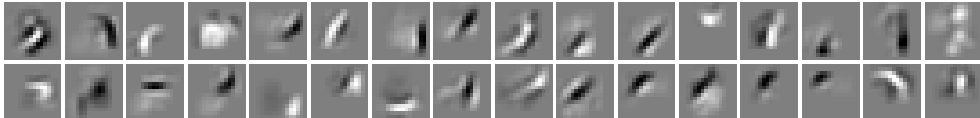
Figure C.1: Computational architecture of a 3-Layers ML-CSC model. In this model  $\gamma_3$  is the only encoded layer,  $\epsilon$  is the representation error. The virtual layers  $\gamma_1$  and  $\gamma_2$  are not explicitly computed, but could be estimated if needed. The feed-back and feed-forward effective dictionary, are factorized into smaller and simpler sparse dictionaries  $D_i$ .  $\gamma_3$  is passed through a non linearity to force sparseness. The level of sparseness is tuned with the  $\lambda_3$  parameter.

## Appendix D. Features extracted by the ML-CSC

(a) ML-CSC first-layer RFs on MNIST



(b) ML-CSC second-layer RFs on MNIST



(c) ML-CSC third-layer RFs on MNIST

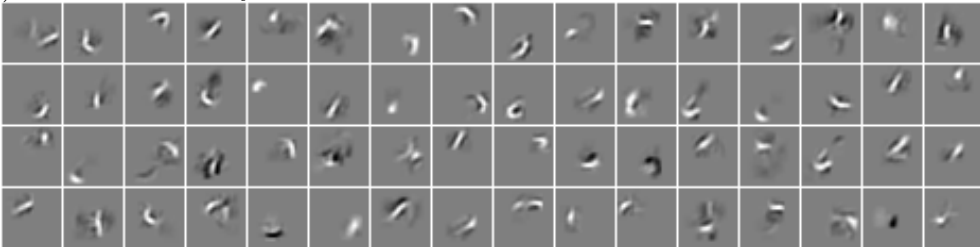


Figure D.1: Features extracted by the ML-CSC after unsupervised training on MNIST. (a) 16 second-layer RFs (randomly selected) of size  $7 \times 7$  pixels, drawn from the effective dictionary  $\mathbf{D}^{(1)}$ . (b) 32 second-layer RFs (randomly selected) of size  $16 \times 16$  pixels, drawn from the effective dictionary  $\mathbf{D}^{(2)}$ . (c) 64 second-layer RFs (randomly selected) of size  $28 \times 28$  pixels, drawn from the effective dictionary  $\mathbf{D}^{(3)}$ .